BER the international journal of bridge engineering management and research

Sensing Skin Technology for Fatigue Crack Monitoring of Steel Bridges: Laboratory Development, Field Validation, and Future Directions

Han Liu[1,*]; Simon Laflamme[1,2]; Jian Li[3,4]; Austin R. J. Downey[5,6]; Caroline Bennett[3]; William N. Collins[3]; Paul Ziehl[5,6]; Hongki Jo[7]; and Michael Todsen[8]

Abstract: A significant number of steel bridges are vulnerable to fatigue cracks, and the timely discovery of damage is critical in ensuring safety and continuous operations. Despite various crack monitoring methods available in the field of structural health monitoring (SHM) to empower real-time feedback, few commercially-available technologies are applicable to the task of discovering new cracks because of the highly localized nature of the sensors. The authors have developed a sensing skin constituted of -soft elastomeric capacitors (SECs). An SEC is a large-area strain gauge that transduces strain into a measurable change in capacitance. It can be easily deployed over large surfaces and thus can be used to discover new fatigue cracks. The technology has been developed and characterized in a laboratory environment over the last decade. It has been recently deployed in the field on a bridge located in Kansas, USA. The aim of this paper is to present and discuss technological updates that were necessary to enable field deployment, with the objective of supporting the field deployment of the cSEC and other SHM technologies. In particular, it reviews the following SEC technology modifications: 1) corrugation of the surface of the dielectric, creating a corrugated SEC or cSEC, to improve sensing performance; 2) development of a dedicated wireless data acquisition system; and 3) improvement of the data fusion algorithm to account for higher signal contamination in the field. After this review, challenges in conducting field deployment are examined. Lastly, a discussion on the path to commercialization is provided.

Author keywords: Structural health monitoring; soft elastomeric capacitor; capacitive sensor board; fatigue; steel bridges

Introduction

Fatigue cracks are one of the primary mechanisms that may compromise the structural integrity of steel bridges.[1] Timely detection, evaluation, and repair of fatigue damage are necessary for ensuring safe and continuous operations by preventing excessive deterioration and catastrophic failures.[2,3] Visual inspection is the most common approach used for fatigue crack detection, but this process relies on the inspector's judgment and thus presents challenges for early-stage hairline-thin crack detection because of low contrast between the crack and the adjacent metallic surface.[4,5] Various nondestructive evaluation technologies have recently been proposed to assist visual inspections. Examples include magnetic particle,[6] ultrasonic,[7,8] computer vision,[9–11] and X-ray imaging.[12] While these approaches are well accepted by the bridge management community, they rely on the use of trained agents, are sporadic, and may be expensive and time-consuming to conduct.

A promising solution is to use structural health monitoring (SHM) technologies to automate the crack discovery and evaluation process by leveraging tailored signal processing and decision-making algorithms.[13,14] However, the use of conventional SHM technologies for fatigue crack discovery is difficult because the most available solutions are too small in size and have one-dimensional sensing capabilities, which makes the discovery of a crack unlikely from a probabilistic perspective,[15] with a few exceptions including acoustic emission technology.[16,17] To address this issue, researchers have proposed large-area electronics (LAE) that can be deployed as a dense sensor network, often termed sensing skin.[18,19] Specific examples of LAE developed for fatigue crack monitoring include piezoelectric sensor/actuator networks,[20] carbon nanotube-based sensing skin,[21] and strain sensing sheets.[22] Compared to commercially available strain sensors, sensing skins provide large area coverage, thus enabling direct damage discovery at pre-determined resolutions over large-scale components.[23,24]

The authors have previously proposed a soft elastomeric capacitor (SEC) technology. The SEC is a flexible, low-cost,

*Corresponding Author: Han Liu. Email: liuhan@iastate.edu
[1]Department of Civil, Construction, and Environmental Engineering, Iowa State University, Ames, IA, USA
[2]Department of Electrical and Computer Engineering, Iowa State University, Ames, IA, USA
[3]Department of Civil, Environmental and Architectural Engineering, The University of Kansas, Lawrence, KS, USA
[4]Department of Electrical Engineering and Computer Science, The University of Kansas, Lawrence, KS, USA
[5]Department of Mechanical Engineering, University of South Carolina, Columbia, SC, USA
[6]Department of Civil and Environmental Engineering, University of South Carolina, Columbia, SC, USA
[7]Department of Civil, Architectural, Environmental Engineering and Mechanics, The University of Arizona, Tucson, AZ, USA
[8]Bridges and Structures Bureau, Iowa Department of Transportation, Ames, IA, USA

compliant, and skin-type strain sensor that transduces strain into a measurable change in capacitance. A new generation of the SEC was recently proposed by texturing the top surface to ameliorate its sensing performance, termed corrugated SEC (cSEC).[25] The cSEC has been characterized and applied for monitoring fatigue cracks in steel compact, C(T), specimens[26] and corner welds,[27] and demonstrated in the field on a bridge located in Kansas, USA.[28] The aim of this paper is to present technological updates that were required to bridge the gap between laboratory studies[25–27] and field deployment.[28] Syntheses of sensor development work in the structural health monitoring community are rarely disseminated, and thus, the novelty of this manuscript resides in summarizing 15 years of research and development that led to a field demonstration. Through this overview of "lessons learned," the authors anticipate supporting further field implementations of new SHM technologies.

Fig. 1 presents an overview of key technological updates that were implemented. These are discussed sequentially in the sections that follow. First, the SEC itself was modified with a corrugated pattern to improve sensing performance in terms of signal-to-noise ratio and resolution, giving rise to the cSEC. Second, a dedicated wireless data acquisition system was designed to read and transmit capacitance data. Third, the signal processing algorithm, originally termed the crack growth index (CGI), was modified to improve accuracy and robustness with respect to real-world traffic loading and environmental noise (now termed "modified CGI"). Fourth, challenges in conducting field validation are reviewed. Fifth, a discussion on a path to commercialization is provided.

Sensing Skin Technology

Soft elastomeric capacitor (SEC)

The SEC is a robust large-area capacitor that transduces strain into a measurable change in capacitance. Its design, fabrication, and sensing principle are described in detail in Laflamme et al.[29] Fig. 2a presents a square-shaped SEC of 76 mm × 76 mm. The technology is a flexible and stretchable parallel capacitor constituted by a dielectric layer sandwiched between conductive plates, as shown in Fig. 2b.

The dielectric layer of the sensor is fabricated by doping titania (TiO_2) particles at 7.5 w% into a block co-polymer matrix of styrene-ethylene/butylene-styrene (SEBS), used to

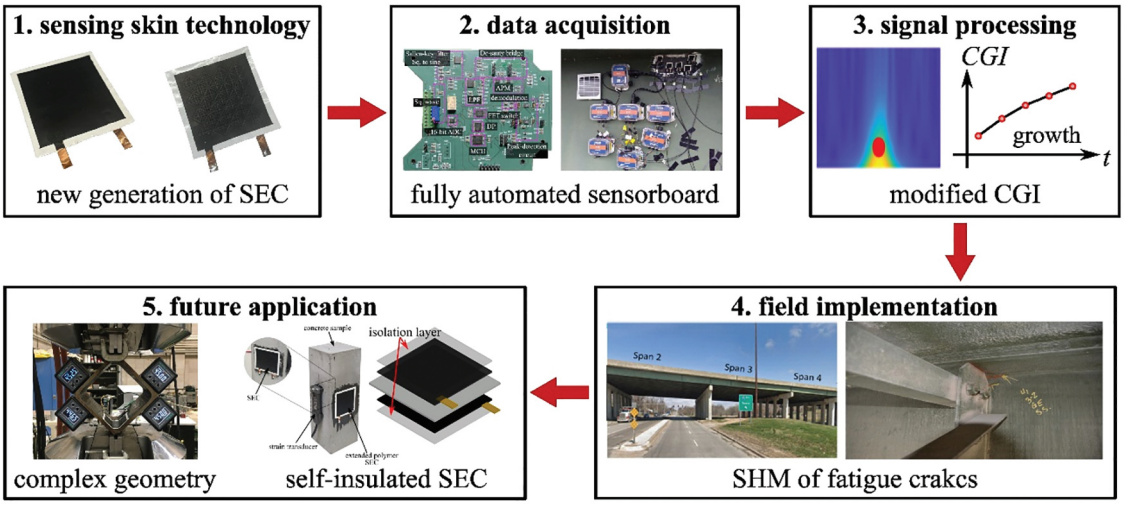

Figure 1. Overview of technological updates enabling field deployment of the SEC technology

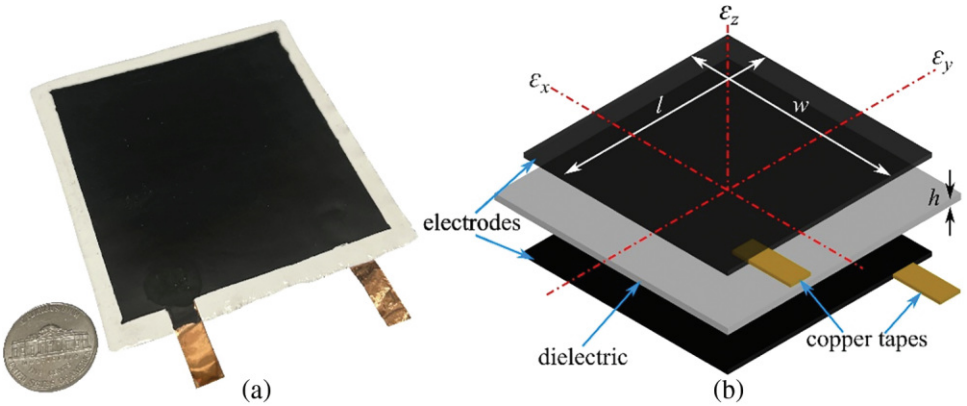

Figure 2. Picture of a 76 mm × 76 mm SEC; and (b) an exploded view of the sensor architecture with key components annotated

increase permittivity and durability. The conductive plates (i.e., electrodes) are also constructed from an SEBS matrix but doped with carbon black particles at 2.5 w% to provide conductivity while improving the stability of SEBS against UV degradation. Two adhesive copper tapes are installed onto the top and bottom electrodes to enable the mechanical connection. Here, the top electrode is used as input to the data acquisition (DAQ) system, and the bottom electrode is used for grounding. The inclusion of the titania and carbon black is critical in providing the sensor with high durability and weatherability protection for field implementation.[30]

The SEC is an excellent technology for fatigue crack detection, localization, and monitoring of metallic structures. It can cover large areas in a networked configuration due to its high scalability arising from the use of readily available, inexpensive raw materials and its simple fabrication process. Its ultra compliance guarantees robustness and durability with respect to fatigue crack quantification and long-term monitoring. Assuming under a low measurement frequency (<1 kHz), the initial capacitance C_0 of the SEC is formulated as:

$$C_0 = e_0 e_r \frac{A}{h} \tag{1}$$

where $e_0 = 8.854\ \text{pFm}^{-1}$ is the vacuum permittivity, e_r is the dielectric permittivity, $A = w \times l$ is the sensing area of the SEC, with w and l being the width and length of the electrode, and h is the thickness of the dielectric, as denoted in Fig. 2b.

When installed over a fatigue crack, the opening and closing of the crack causes a geometric deformation of the sensor, thus provoking a measurable change in its capacitance. It is a remarkable fact that prior studies demonstrated that the sensors' signal can detect cracks in its vicinity, not only those located underneath.[9] Its electromechanical behavior, under the assumption of in-plane stress when deployed onto a steel surface, can be modeled as:[26]

$$\frac{\Delta C}{C_0} = \frac{1}{1-\nu}(\varepsilon_x + \varepsilon_y) \tag{2}$$

where ΔC is the measured differential change in capacitance, ν is the Poisson's ratio with $\nu \approx 0.49$ at small strain,[25] $\frac{1}{1-\nu}$ is the gauge factor λ, and ε_x and ε_y are the strains in the x and y directions, respectively. Eq. (2) reveals that ΔC varies linearly with the in-plane strains ε_x and ε_y, and thus its signal can be used to measure fatigue crack growth. That relationship in Eq. (2) assumes full adhesion of the sensor onto the monitored surface. When subjected to a fatigue crack, the sensor stretches over the opening of the crack and measures the localized strain that significantly boosts the signal's magnitude.

Corrugated soft elastomeric capacitor (cSEC)

The design of the SEC has been altered recently to improve signal stability and sensitivity to facilitate field implementation. This was done by corrugating the top surface of the

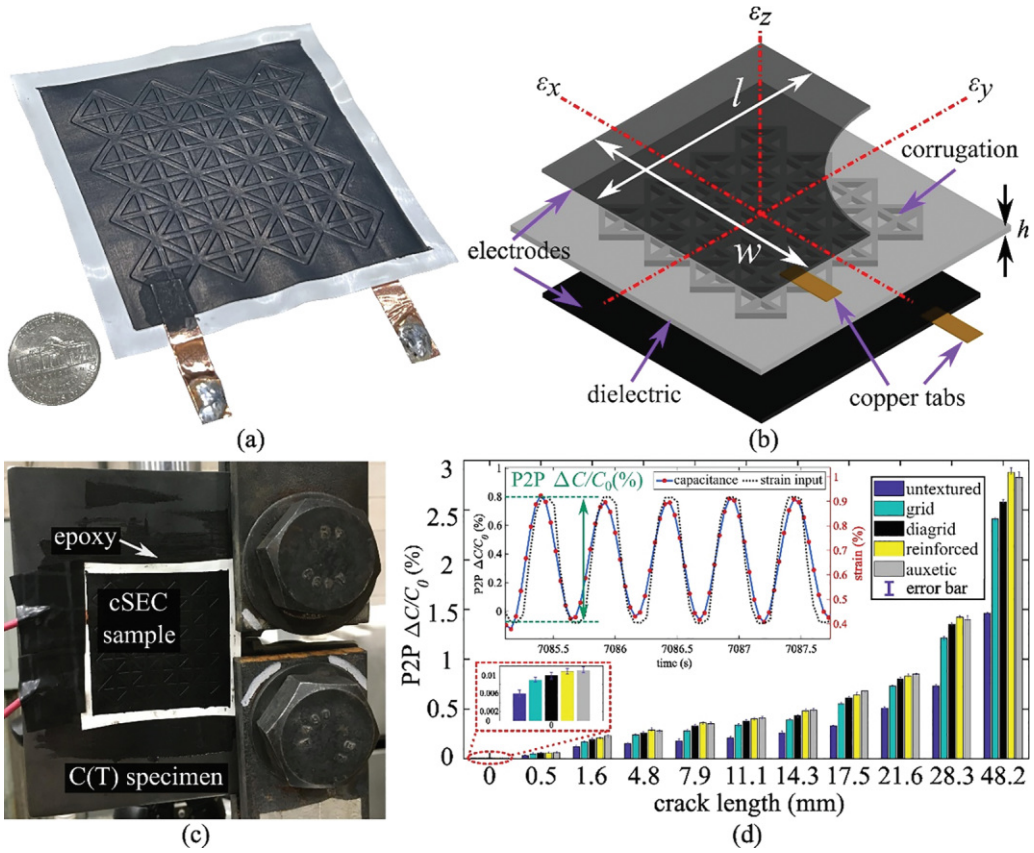

Figure 3. A cSEC with reinforced diagrid pattern; (b) schematic of the cSEC; (c) experimental setup showing a cSEC on a C(T) specimen; and (d) typical time series results of the P2P versus crack length under different corrugation patterns

dielectric to tune the sensor's stiffness, resulting in lowering the sensor's Poisson's ratio and improving its mechanical stability. This new generation cSEC is shown in Figs. 3a and 3b. Its design, fabrication process, and electromechanical model were reported in Liu et al.[25] Experimental results conducted on C(T) steel specimens confirmed that the cSEC produces a net improvement in the sensing performance in terms of linearity, sensitivity, resolution, and accuracy.[26] A key result is presented in Fig. 3d for the experimental setup shown in Fig. 3c. Four corrugation patterns were investigated (symmetric grid, diagonal diagrid, reinforced diagrid, and re-entrant hexagonal honeycomb) and benchmarked against the original SEC, which was untextured. Experimental results were evaluated by cross-comparing the three-sample averaged peak-to-peak (P2P) amplitudes of the signals between each pattern over different crack lengths. Results are graphed in Fig. 3d. The cSEC exhibited an increase in the P2P amplitudes of approximately 50% to 100% when compared to the untextured SEC applied over various crack lengths. The reinforced diagrid pattern, depicted in Figs. 3a and 3b, was selected for field implementation because it 1) outperformed most other patterns in terms of sensitivity to crack opening and 2) was a symmetric design, thus making it easier to deploy in the field.

Data Acquisition

Experimental works on the SEC and cSEC used a wired commercial capacitance measurement device termed PCAP (model PCAP02). However, the use of a wired DAQ impedes the practicality of any field application because of added difficulties in installation, costly cabling, inefficient data transmission, high energy dissipation, and poor accessibility.[31] To this end, a dedicated, wireless DAQ was developed, consisting of a capacitive strain sensor board (c-strain board) integrated with a smart sensor platform (Xnode). The c-strain board is a De Sauty bridge-based capacitive strain sensing interface that can transform the strain-induced dynamic capacitance changes of the SEC into analog voltage signals.[32] Yet, the precise alternating current (AC)-bridge balancing, signal amplification control, and shunt calibration process associated with the c-strain sensor board operation were originally achieved manually, which also constitutes an important limitation to field deployments.[33] Fig. 4a shows the picture of the automated c-strain sensor board.

The newly developed capacitive strain sensing node was built by integrating the automated c-strain sensor board with a commercial wireless smart sensor platform, Xnode. The Xnode is the wireless transmission node that consists of a processor board, radio and power board, and the 24-bit data acquisition board in a layer-up configuration, as shown in Fig. 4b. It is known as a versatile wireless sensor system through its various functionalities: flexible interface with external sensors, low power radio transceiver (Atmel AT 86RF233), onboard dual-core signal processing (ARM cortex M0/M4), optional high quality of long-range wireless communication through 4G LTE module (Sierra Wireless HL7588 LTE-CAT4), expandable data storage, 24-bit analog-to-digital conversion (ADS131E8), user-configurable middleware software library, and so on Oliva et al.,[34] Hoang et al.,[35] Fu et al.,[36] Fu et al.[37] The Xnode also has a high-capacity lithium-ion rechargeable battery, which is here equipped with solar panel support to provide an autonomous energy source in the field (inset of Fig. 10d).

The performance of the developed wireless capacitance sensor in combination with the SEC was evaluated through free-vibration tests using a cantilever beam. The experimental setup is presented in Fig. 5a. Two cSECs of similar initial capacitance were adhered onto a steel plate using epoxy (JB Weld), and a foil-type strain gauge (OMEGA kFH-3-120-C1-11L3M3R) was installed between them for comparison. The automated c-strain sensor board and the wired commercial capacitance measurement device PCAP (PCAP02) were subsequently connected to the same SEC for data collection at 100 Hz, and the data from the foil-type strain gauge was recorded using a National Instrument CompactDAQ chassis (cDAQ-9178) with the NI9235 module at a sampling frequency of 2 kHz. The cantilever plate was subjected to free vibration generated by pushing down and releasing the free end of the beam, introducing about 400 micro-strains measured by the strain gauge, which was within the effective strain range experienced by a cSEC monitoring fatigue cracks in the steel. Fig. 5b presents the strain measured from the strain gauge and compares the signal collected by the c-strain sensor board and PCAP02. It can be noticed that

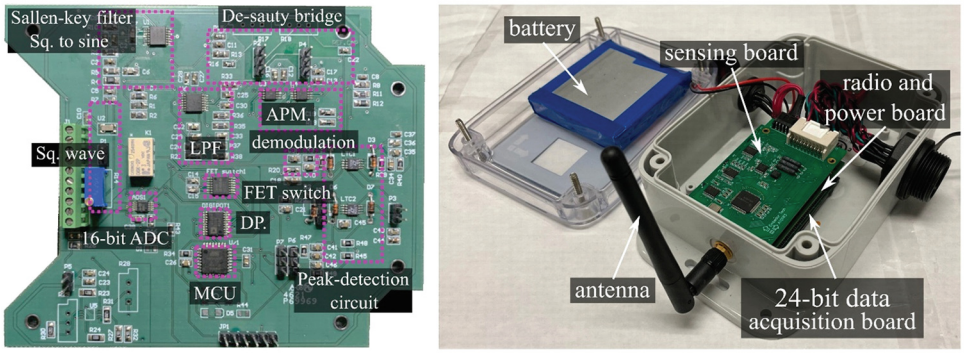

(a) (b)

Figure 4. Wireless capacitive sensor node: (a) automated c-strain sensor board; and (b) Xnode smart sensor platform

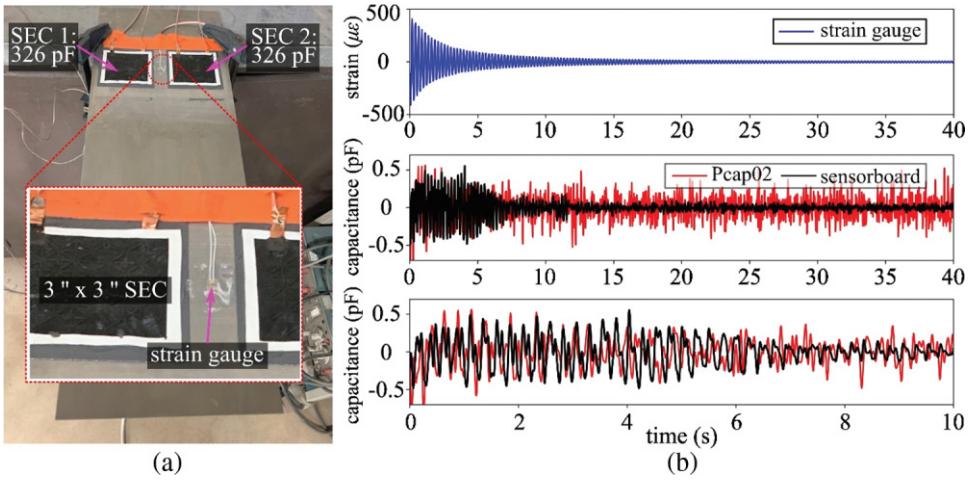

Figure 5. (a) Cantilever plate setup for free vibration test; and (b) experimental results comparing signal measured from strain gauge (top), PCAP02 (middle), and sensor board (bottom)

both the sensor board and PCAP02 showed a very similar trend at the initial stage when the vibration amplitude was large. The sensor board's signal decayed was more similar to that of the strain gauge compared to the PCAP02 signal, exhibiting approximately 34% lower measurement noise. The fluctuation of the sensor board's signal after 10 seconds can be attributed to electromagnetic noise. More details about the c-strain sensor board and associated experimental tests can be found in Jeong et al.[33]

Signal Processing

A crack growth index (CGI) was initially developed to fuse SEC signals into a metric related to fatigue crack length. The CGI was taken as the ratio between the power spectral density (PSD) peak of $\Delta C(t)$ and the applied $F(t)$ to normalize $\Delta C(t)$ (i.e., removing the impact of the changing traffic load magnitude), making the CGI an input-independent metric.[38] Note that $F(t)$ can be any signal that relates to the input, for example the reading of a strain gauges measuring the axial strain of a member of the cross-frame of a girder bridge provoked by the passage of a vehicle.[39]

The original CGI works well for the proof-of-concept laboratory tests, where the $\Delta C(t)$ and $F(t)$ were both sinusoidal signals.[38] The CGI was further improved by introducing a moving-average filter to smooth the PSD curves to deal with signals with randomized frequencies and amplitudes.[40] However, traffic-induced bridge response measurements in the real world resemble impulse-like signals induced by individual vehicle passing, as opposed to sinusoidal signals, and they are subject to noise contamination, such as low-frequency drift likely arising from the intrinsic electrical behavior exhibited by many sensors fabricated using hyper-elastic polymers,[41,42] as exemplified in Fig. 12 that compares sensor measurements collected in the laboratory and in the field. These issues limited the success of using the Fourier transform in the CGI. Thus, the CGI was modified to utilize, instead, wavelet transform to accurately detect the amplitude of each individual impulse event that tracks potential fatigue crack growth under traffic load. The developed new CGI algorithm presents a complete system for long-term fatigue crack monitoring in the field with the procedure diagrammed in Fig. 6 and is conducted as follows:

First, traffic detection is conducted using an accelerometer installed on the bridge. When the acceleration is above a user-defined threshold, signals from the cSECs are collected, as well as that from a strain gauge, the latter of which is used to indirectly obtain $F(t)$. Second, a continuous wavelet transform using Morse wavelet is conducted on the signal and peaks in the data are identified. See references[43,44] for additional details on the wavelet transform technique. The signal

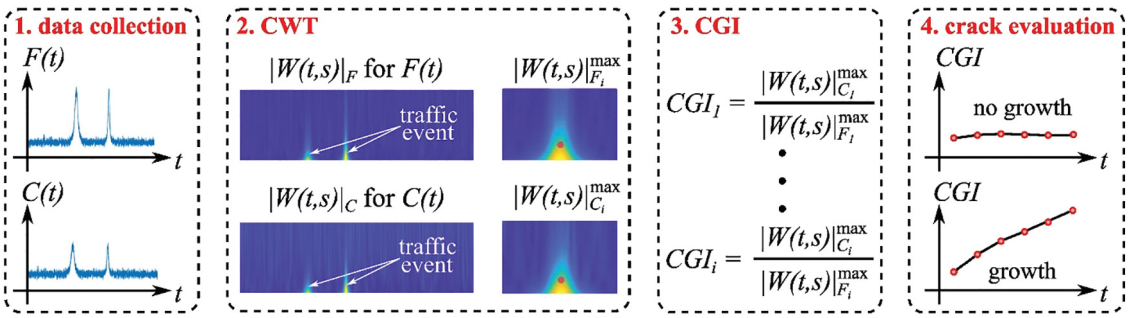

Figure 6. Workflow of the modified CGI algorithm

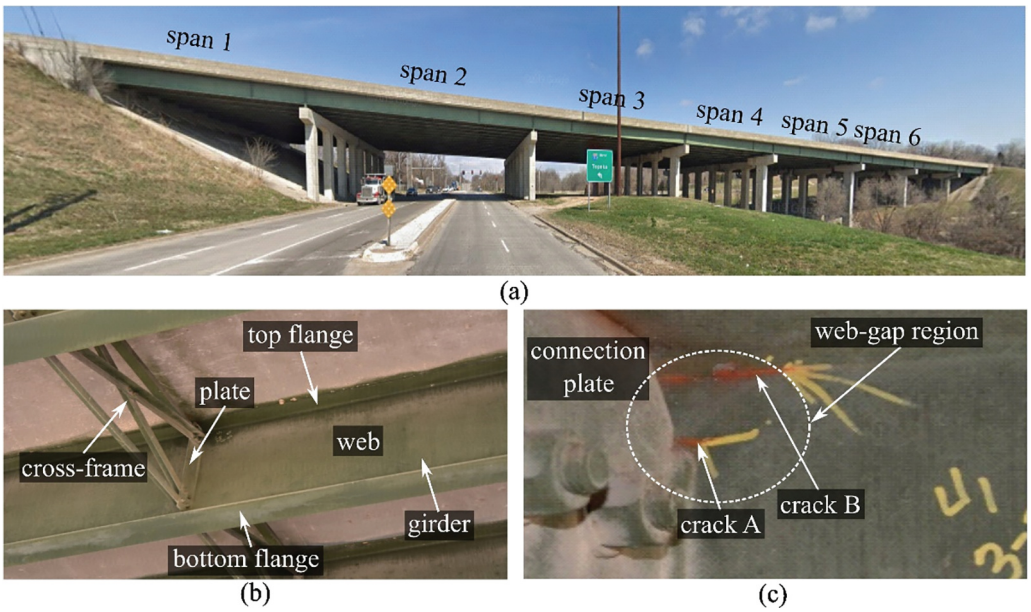

Figure 7. I-70 bridge: (a) span layout of the bridge; (b) cross-frame between the adjacent girders; and (c) detail of the web-gap region with distortion-induced fatigue cracks (adapted from Taher et al.[28])

is further processed within windows of interest $\text{WOI}_i = [t_i - t_d, t_i + t_d]$, where $i = 1, 2, \ldots, n$ represents the number of detected peaks n, and t_d is a time window separating peaks. Third, the maximum values from the capacitance $|W(t,s)|_{C_i}^{\max}$ and input $|W(t,s)|_{F_i}^{\max}$ signals within each WOI_i are extracted and represent the detected traffic events. An example of such an event is indicated by a pink dot in Fig. 6 (step 2). Third, the CGI is taken as:

$$\text{CGI}_i = \frac{|W(t,s)|_{C_i}^{\max}}{|W(t,s)|_{F_i}^{\max}} \tag{3}$$

Fourth, crack size and its growth are determined through a spatio-temporal study of the CGIs. Laboratory results reported in Kong et al.[38] showed a linear relationship between the CGI and the fatigue crack length. Therefore, the CGI would gradually increase if the crack grows. Otherwise, the CGI remains constant if there is no crack growth.

Field Implementation

The SEC was deployed in the field on a multi-span steel highway bridge. The bridge (Fig. 7a), designated 70-105-41732-128 (eastbound), is located at the intersection of N. 57th Street and I-70 highway near Kansas City, Kansas. According to the inspection report released by the Kansas Department of Transportation (KDOT), the bridge has multiple fatigue cracks. Fig. 7b shows a typical cross-frame (Span 3) connected to the girder web using a transverse connection plate. Span 3 was monitored, which had two distortion-induced fatigue cracks on one of the girders, as shown in Fig. 7c, where crack A is near the web-gap region along the weld between the transverse connection plate and the girder web, and crack B is along the weld toe between the top flange and web.

The field installation process (diagramed in Fig. 8) occurred as follows. First, SECs were installed on the web-gap region directly over the fatigue cracks, and foil-type strain gauges (FLA-5-11-3LJCT) were installed on the cross-frame to capture the out-of-plane force indirectly $F(t)$ acting on the web-gap region exerted by the cross-frame, proportional to the traffic loading. A direct current (DC) Wheatstone bridge circuit module, shown in Fig. 9a, was used to convert the strain ε to a voltage signal. The c-strain sensor board and DC Wheatstone bridge were connected to the SECs and strain gauge to measure analog voltage signals relating to $\Delta C(t)$ and $F(t)$. In this application, the $F(t)$ value corresponding to a 30 $\mu\varepsilon$ was selected as the event detection threshold, here, by heavy vehicles. A minimum peak distance $t_d = 1.3$ s was selected to avoid closely spaced peaks that would likely be caused by noise.

Second, the Xnode used in this work was equipped with an 8-channel 24-bit AD converter, in which the first three channels were used for the onboard tri-axial accelerometer, and the remaining five channels were used for external sensors such as the strain gauge and SECs. A breakout box, shown in Fig. 9b, was employed to connect both the c-strain sensor board and DC Wheatstone bridge module to the Xnode to split a multi-cable line into eight compound connectors, ensuring robust connections for power supply and receiving external sensor voltage signals, and supporting integration testing and troubleshooting processes. The Xnode was also equipped with a low-power trigger accelerometer (ADXL362 by Analog Devices) to enable event-triggered sensing mode with a predefined acceleration threshold. This event-triggered sensing mode is used to tailor data collection to meaningful events and to optimize the Xnode power usage. In this application, acceleration thresholds of 150 and 250 mg were selected depending on the

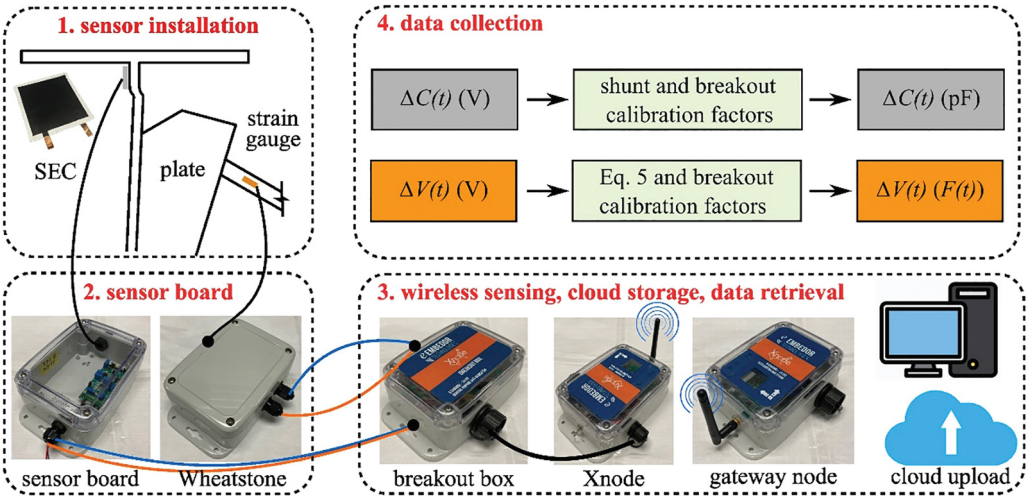

Figure 8. Developed in-field fatigue crack sensing flow chart

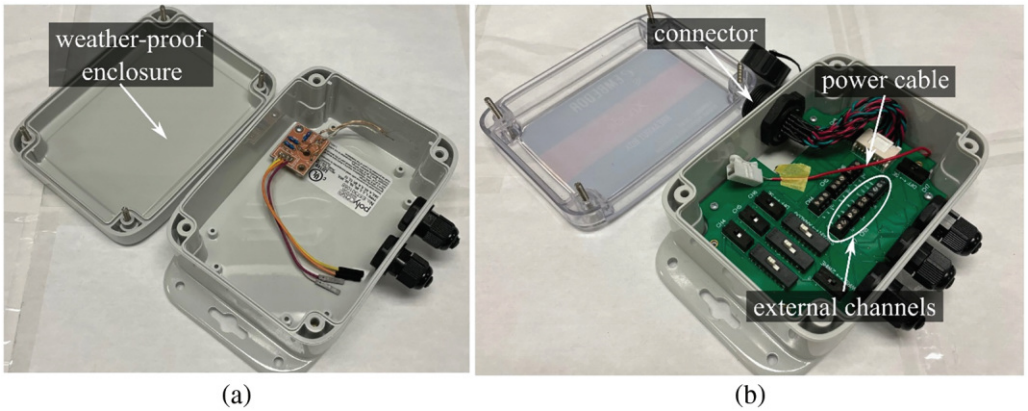

Figure 9. Pictures of (a) the DC Wheatstone bridge module; and (b) the breakout box

stiffness of the structural components to ensure that only significant loading events were collected.

Third, a cellular gateway node was equipped with a 4G-LTE modem to receive the signals from the Xnode and to upload data to the cloud server for wireless communications and remote data retrieval.[35] Fourth, cloud data was accessed using a PC, and the desired $\Delta C(t)$ and $F(t)$ were obtained by applying the shunt calibration coefficients along with the breakout box factor on the voltage signals of $C(t)$ and $V(t)$, respectively.

Structural surfaces shown in Fig. 10a were sanded and cleaned to remove paint and debris prior to sensor installation. Subsequently, a thin layer of an off-the-shelf bi-component epoxy (JB Weld) was applied over the crack on the web-gap-region, and SECs adhered to the epoxy layer (Fig. 10b). Foil-type strain gauges were installed on a diagonal member (Fig. 10c) of the cross-frame with the Wheatstone bridge configuration using adhesive and coating. Fig. 10d is an annotated picture showing the installed sensor network under the first girder of Span 3, and the inset shows the facia side of the girder with cSECs installed. All components of the integrated system, except the capacitive sensor board, were deployed on the bottom flange of the girder. The capacitive sensor board was installed close to the cSEC to reduce cable length, thus minimizing the noise from capacitance measurement. Additionally, data analysis focuses on extracting the peaks associated with dynamic responses during a short period of time, which has a minimum impact from temperature change. After installation, AC bridge balancing and a two-step Shunt calibration were performed on the capacitive sensor board. All devices and sensor boards, except the cSECs, in this application were packaged in a weather-proof enclosure to improve durability and offer protection against environmental hazards. Prior work showed that the SEC was robust with respect to aging, attributable to the use of titania and carbon black, where the titania doped dielectric layer provides the sensor with a level of durability against weathering, while the carbon black inclusions to the conductive layer improved the sensor's durability and weatherability protection.[30] The bridge is not equipped with any other monitoring system, and the research team plans to conduct an ultrasonic test in the near future to verify the length of the fatigue crack measured by a cSEC. Data collection is scheduled to continue throughout the upcoming years.

A large-scale, non-skewed bridge girder connection was tested in a laboratory environment to validate field sensing data.[38] The test reproduced distortion-induced fatigue

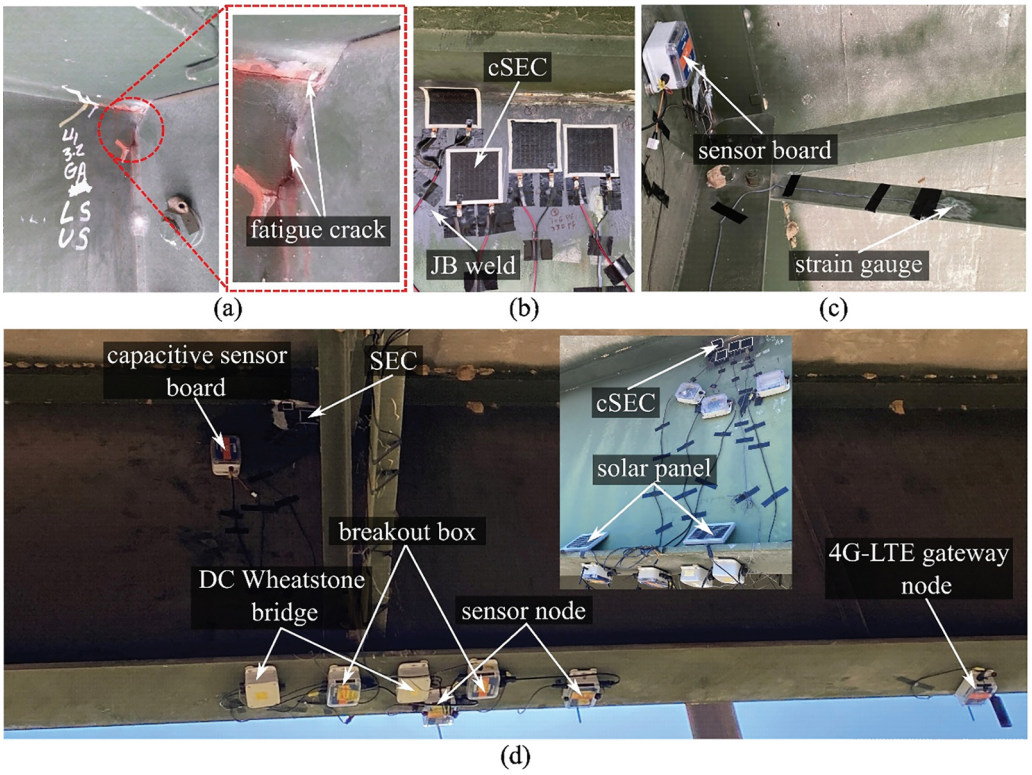

Figure 10. Installation of the sensor network: (a) fatigue crack location; (b) cSEC; (c) strain gauge location; and (d) overall wireless sensor network showing key hardware (adopted from Taher et al.[28] with the inset showing the facia side of the girder)

cracks in a structural system similar to that of the bridge, with the difference being that the girder to cross-frame connection is a simplified subassembly of the entire bridge system without considering the effect of the bridge deck. As shown in Fig. 11a, the bridge girder was mounted upside-down to simulate the boundary conditions due to the deck. A cross-frame was connected to the girder through the connection plates, with a 90° skew angle between the cross-frame and girder. SECs were deployed at the bottom web-gap region to assess fatigue cracks, as shown in Fig. 11b, and foil-type strain gauges were installed on the top horizontal cross-frame member to indirectly capture load $F(t)$. An actuator was vertically installed at the far end of the cross-frame to apply fatigue load on the girder. This setup was designed to allow vertical movement only by preventing lateral movement and rotation of the girder web. A 0.5 Hz harmonic excitation with a constant load range of 2.2 to 25.5 kN (0.5 to 5.75 kip) was applied (Fig. 12a). This load is under a symmetric distribution (±2.62 kip) in order to consider the reversal behavior of the traffic load in the field. SECs were removed after a total of 18,900 fatigue cycles to inspect the newly initiated fatigue crack beneath the sensor. Laboratory

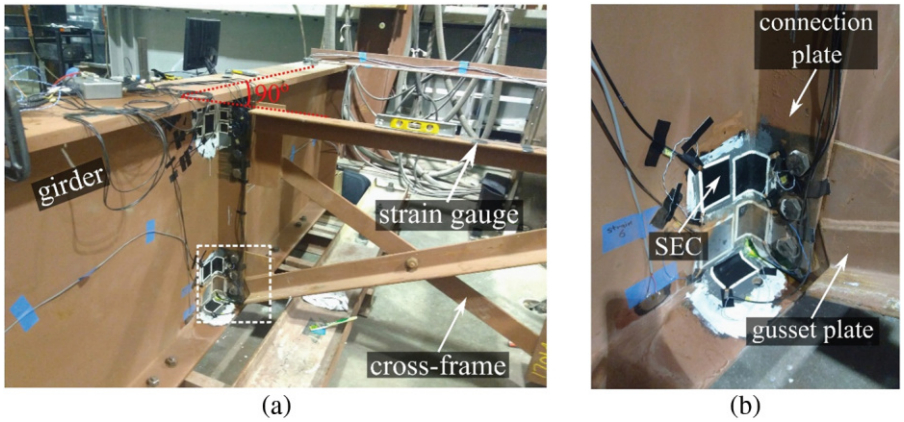

Figure 11. (a) Laboratory setup showing the non-skewed bridge girder and cross-frame connection; and (b) zoom on the installed SECs (adapted from Kong et al.[38])

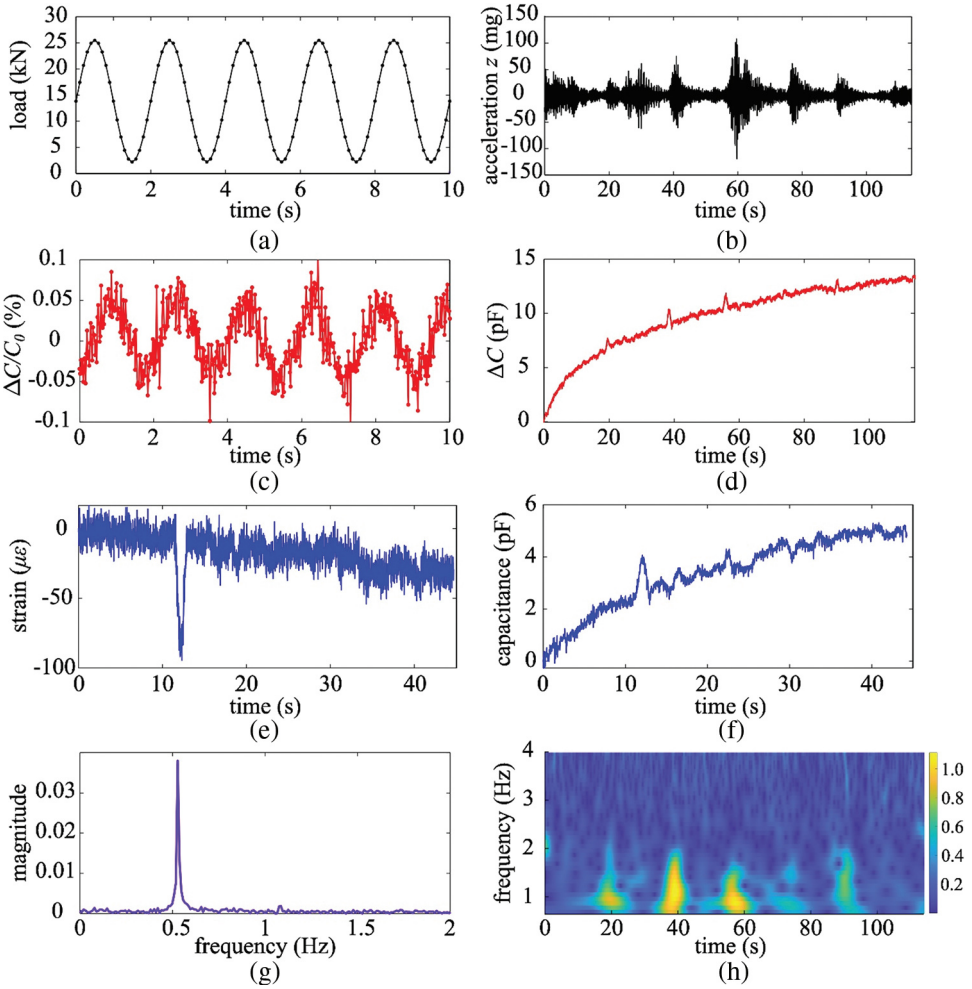

Figure 12. (a) Compression load applied on the laboratory non-skewed bridge girder connection; (b) acceleration measurements collected under multiple impulse traffic events; (c) time series plots of relative change in capacitance $\Delta C(t)/C_0$ measured from the laboratory non-skewed bridge girder; (d) time series plot of change in capacitance $\Delta C(t)$ measured from field bridge girder; (e) strain measurements collected by the strain gauge; (f) strain measurement collected by the SEC; (g) frequency spectrum of the SEC applied on laboratory bridge girder; and (h) CWT spectrogram plot of the magnitude of capacitance $|W(t, s)|_{C_i}$ signal collected from the field bridge girder

results, presented in Kong et al.,[40] used the original CGI, and demonstrated a linear relationship between the CGI and the number of actuation cycles once the fatigue crack was initiated, as shown in Fig. 13.

Results and Discussion

Fig. 12 presents key differences between laboratory-acquired data (left) and field-acquired data (right). In the field, the signal is that of an SEC installed at the bottom web-gap region of the laboratory bridge girder and located in front of the crack propagation path. The capacitance signal acquired in the laboratory environment (Fig. 12c) was typically acquired from a harmonic loading (Fig. 12a). In comparison, the capacitance data (Fig. 12d) acquired from field events (Fig. 12b) contains impulsive traffic events, is noisy, and exhibits a nonlinear DC component that may be attributable to a thermal effect when loading the sensor.

Figs. 12e and 12f show an example of the raw data measured by the strain gauge installed on the cross frame and the SEC installed in the web-gap region during a large impulsive event caused by traffic loading. A good match of the signal peaks is visible between 11 and 13 s, which also corresponds to the peak acceleration measured by the accelerometer. Figs. 12g and 12h compare Fourier and Wavelet transforms from the laboratory and field signals, respectively, illustrating the differences in signal complexity. The field signal is the result of multiple vehicular loading events, at 20, 40, 58, and 91 seconds. Fig. 12e shows a fundamental frequency peak at 0.5 Hz that can clearly be observed, consistent with the input loading frequency. For the field data, the capacitance time series was filtered using detrending, high-pass filtering, and low-pass filtering to remove the low-frequency drift and high-frequency noise in the data, respectively. The cutoff frequencies of the high-pass and low-pass filters were 0.05 Hz and 4 Hz, respectively. The resulting CWT plots (Fig. 12f) exhibit concentrated signal energy in both time

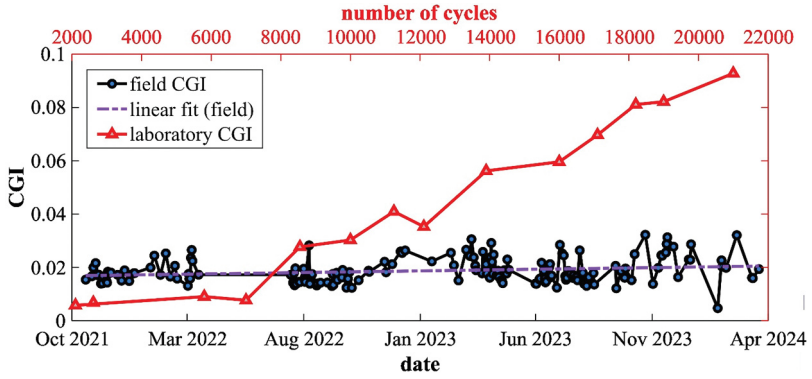

Figure 13. Comparison of averaged field CGI with the laboratory CGI

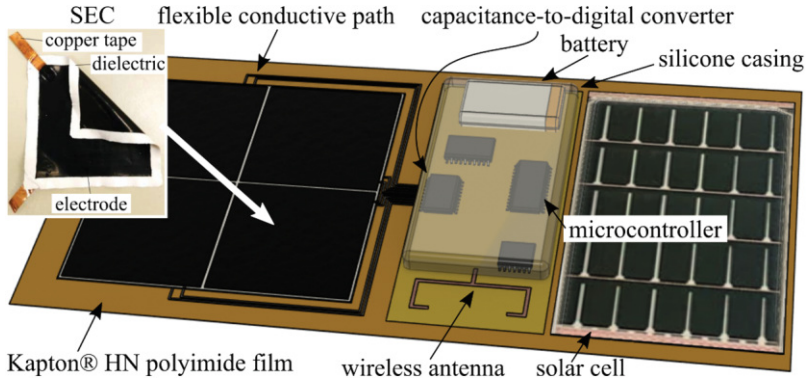

Figure 14. Visualization of an SEC-based, fully integrated sensing skin constructed as a printed hybrid flexible electronic device that will enable the fast and efficient deployment of the sensor for the monitoring of civil infrastructure

and frequency during traffic events, obtained by using the modified CGI algorithm illustrated in Fig. 6.

The modified CGI was extracted in the field from mid-October 2021 to mid-March 2024. A total of 168 datasets containing 1035 impulse events were collected and processed. These CGIs are plotted in Fig. 13. The presented field CGI are mean values averaged over one to two days using a minimum of two events. It can be observed that the linear fit of the field CGI has a positive slope, indicating the CGI slightly increased and that the fatigue crack propagated further during the monitoring period. Some fluctuations may be attributed to seasonal effects, whereas the magnitude of the crack opening with traffic is expected to vary with the bridge's temperature. This investigation is left to future work. Fig. 13 also compared field CGI values against those obtained from laboratory tests (using a Fourier transform) reported in Kong et al.,[38] where an array of SECs was used to cover a full-scale bridge girder to cross-frame welded connection to construct a CGI mapping the progression of a fatigue crack. The laboratory CGI increases starting at approximately 7000 cycles when the crack began initiating and then increases linearly with the number of cycles, correlating with crack length. It follows that the field CGI corresponds to an early crack size, as expected.

Recommendations for Future Work

Preliminary results obtained from the field deployment presented in this paper have demonstrated the successful transition of the SEC technology from the laboratory to the field environment, constituting a major step towards widespread deployment. The next major gap will be that of commercialization, where the technology will require another round of major updates to allow for a cost-effective and easy installation. The vision is a flexible and stretchable product that can be easily adhered to critical surfaces. To do so, improved fabrication techniques are needed to facilitate the integration of micro- and nano-particles in the polymer matrix, produce large sheets, and perhaps even update the polymer mix itself to eliminate the need for any solvent. This can be possible, for example, through the adoption of roll-to-roll manufacturing and the use of silicones. Also, the produced sheets of cSECs will require the integration of hardware and the minimization of hard wires. This includes the integration of flexible interconnects, and the development of strategies to join flexible, stretchable, and hard substrates.

The authors propose a possible path to bridging this gap to commercialization through the development of a fully integrated sensing skin.[45–47] The vision for such a sensing skin is shown in Fig. 14. It consists of SECs either attached or fabricated from a base film onto which the required

electronics for data acquisition, processing, and transmission are also adhered. This self-contained printed hybrid flexible electronic sensor would form the backbone of a decentralized network of crack-monitoring flexible sensors. Printed hybrid flexible electronics are a type of printed flexible electronic that include semiconductor devices to expand the capabilities of printed flexible electronics beyond just conductive traces.[48] Aspects of these flexible electronics would be produced through additive manufacturing, reducing assembly cost and allowing for the rapid manufacturing of custom sensor arrangements based on a specific monitoring need.

Conclusion

This paper reported technological updates that were required to enable the field deployment of a sensing skin, termed soft elastomeric capacitor (SEC), developed for fatigue crack discovery and monitoring. Technological updates included: 1) corrugation of the surface of the dielectric, creating a corrugated SEC or cSEC, to improve sensing performance; 2) development of a dedicated wireless data acquisition system; and 3) improvement of the data fusion algorithm to account for the nature of traffic loading and higher signal contamination in the field.

In particular, it was found that the cSEC offered improved sensing properties compared to the original SEC through a higher signal-to-noise ratio and better linearity and sensitivity to strain. This was attributable to the corrugation adding lateral stiffness. The dedicated data acquisition system included a data readout circuit paired with an Xnode for wireless transmission. The data fusion algorithm, termed crack growth index (CGI), was modified by using a continuous wavelet transform instead of a Fourier transform to detect and isolate vehicular events and improve robustness with respect to noise.

Challenges in field deployment were also presented. Importantly, a method had to be developed to assess field performance. A large-scale laboratory setup was constructed to mimic field deployment, and laboratory-acquired CGIs were compared against those obtained in the field. The comparison of results showed good agreement and thus demonstrated the success of the field deployment. Lastly, a path to commercialization was discussed. Namely, the technology will require another round of important updates to enable the production of large sensing sheets with integrated flexible electronics.

Acknowledgments

The authors gratefully acknowledge the financial support of the Departments of Transportation of Iowa, Kansas, South Carolina, and North Carolina through the Transportation Pooled Fund Study TPF-5(449).

Data Availability Statement

The data that support the findings of this study are available from the corresponding author upon reasonable request.

Disclaimer

The statements, opinions, and data contained in all publications are solely those of the individual author(s) and contributor(s) and not of the editor(s).

Supplemental Materials

This paper does not include any supplemental materials. The information and findings presented in the main text constitute the entirety of the content related to the research study.

References

[1] Campbell FC. *Fatigue and Fracture Understanding the Basics*. ASM International; 2012.

[2] Biezma MV, Schanack F. Collapse of steel bridges. *J Perform Constr Facil*. Oct 2007;21(5):398–405.

[3] Haghani R, Al-Emrani M, Heshmati M. Fatigue-prone details in steel bridges. *Buildings*. Nov 2012;2(4):456–476.

[4] Dorafshan S, Campbell LE, Maguire M, et al. Benchmarking unmanned aerial systems- assisted inspection of steel bridges for fatigue cracks. *Transp Res Rec: J Transp Res Board*. Mar 2021;2675:154–166.

[5] Campbell LE, Connor RJ, Whitehead JM, et al. Benchmark for evaluating per- formance in visual inspection of fatigue cracking in steel bridges. *J Bridge Eng*. Jan 2020;25.

[6] Zolfaghari A, Zolfaghari A, Kolahan F. Reliability and sensitivity of magnetic particle non- destructive testing in detecting the surface cracks of welded components. *Nondestruct Test Eval*. Jan 2018;33(3):290–300.

[7] Jeon I, Lim HJ, Liu P, et al. Fatigue crack detection in rotating steel shafts using noncontact ultrasonic modulation measurements. *Eng Struct*. Oct 2019;196:109293.

[8] Sampath S, Sohn H. Detection and localization of fatigue crack using nonlinear ultrasonic three-wave mixing technique. *Int J Fatig*. Feb 2022;155:106582.

[9] Kong X, Li J. Vision-based fatigue crack detection of steel structures using video feature tracking. *Comput-Aided Civil Infrastruct Eng*. Feb 2018;33:783–799.

[10] Dellenbaugh L, Kong X, Al-Salih H, et al. Development of a distortion-induced fatigue crack characterization methodology using digital image correlation. *J Bridge Eng*. Sep 2020;25.

[11] Mojidra R, Li J, Mohammadkhorasani A, et al. Vision-based fatigue crack detection using global motion compensation and video feature tracking. *Earthq Eng Eng Vibr*. Jan 2023.

[12] Qian W, Wu S, Wu Z, et al. In situ x-ray imaging of fatigue crack growth from multiple defects in additively manufactured AlSi10mg alloy. *Int J Fatig*. Feb 2022;155:106616.

[13] Lynch JP, Farrar CR, Michaels JE. Structural health monitoring: technological advances to practical implementations [scanning the issue]. *Proc IEEE*. Aug 2016;104(8):1508–1512.

[14] Sony S, Laventure S, Sadhu A. A literature review of next-generation smart sensing technology in structural

health monitoring. *Struct Control Health Monit*. Jan 2019;26(3):e2321.
[15] Kharroub S, Laflamme S, Song C, et al. Smart sensing skin for detection and localization of fatigue cracks. *Smart Mater Struct*. May 2015;24(6):065004.
[16] Yan Y, Shen Y, Cui X, et al. Localization of multiple leak sources using acoustic emission sensors based on MUSIC algorithm and wavelet packet analysis. *IEEE Sens J.*. Dec 2018;18(23):9812–9820.
[17] Ai L, Zhang B, Ziehl P. A transfer learning approach for acoustic emission zonal localization on steel plate-like structure using numerical simulation and unsupervised domain adaptation. *Mech Syst Signal Process*. Jun 2023;192(9):110216.
[18] Wang Y, Qiu L, Luo Y, et al. A stretchable and large-scale guided wave sensor network for aircraft smart skin of structural health monitoring. *Struct Health Monitor*. Jun 2019;20(3):861–876.
[19] Yan J, Downey A, Cancelli A, et al. Concrete crack detection and monitoring using a capacitive dense sensor array. *Sensors*. Apr 2019;19(8):1843.
[20] Gresil M, Yu L, Shen Y, et al. Predictive model of fatigue crack detection in thick bridge steel structures with piezoelectric wafer active sensors. *Smart Struct Syst*. 2013.
[21] Ahmed S, Schumacher T, Thostenson ET, et al. Performance evaluation of a carbon nanotube sensor for fatigue crack monitoring of metal structures. *Sensors*. Aug 2020;20:4383.
[22] Yao Y, Glisic B. Detection of steel fatigue cracks with strain sensing sheets based on large area electronics. *Sensors*. Apr 2015;15(4):8088–8108.
[23] Liao Y, Zhou P, Pan D, et al. An ultra-thin printable nanocomposite sensor network for structural health monitoring. *Struct Health Monit*. Jul 2019;20:894–903.
[24] Wang Y, Hu S, Xiong T, et al. Recent progress in aircraft smart skin for structural health monitoring. *Struct Health Monit*. Dec 2021;21:2453–2480.
[25] Liu H, Yan J, Kollosche M, et al. Surface textures for stretchable capacitive strain sensors. *Smart Mater Struct*. Sep 2020;29:105037.
[26] Liu H, Laflamme S, Li J, et al. Investigation of surface textured sensing skin for fatigue crack localization and quantification. *Smart Mater Struct*. Sep 2021;30:105030.
[27] Liu H, Laflamme S, Li J, et al. Investigation of textured sensing skin for monitoring fatigue cracks on fillet welds. *Meas Sci Technol*. May 2022;33:084001.
[28] Taher SA, Li J, Jeong J-H, et al. Structural health monitoring of fatigue cracks for steel bridges with wireless large-area strain sensors. *Sensors*. Jul 2022;22(14):5076.
[29] Laflamme S, Saleem HS, Vasan BK, et al. Soft elastomeric capacitor network for strain sensing over large surfaces. *IEEE/ASME Trans Mechatron*. Dec 2013;18:1647–1654.
[30] Downey A, Pisello AL, Fortunati E, et al. Durability and weatherability of a styrene-ethylene-butylene-styrene (SEBS) block copolymer-based sensing skin for civil infrastructure applications. *Sens Actuators A: Phys*. Jul 2019;293:269–280.
[31] Spencer B, Park J-W, Mechitov K, et al. Next generation wireless smart sensors toward sustainable civil infrastructure. *Proc Eng*. 2017;171:5–13.
[32] Jeong J-H, Xu J, Jo H, et al. Development of wireless sensor node hardware for large-area capacitive strain monitoring. *Smart Mater Struct*. Nov 2018;28:015002.
[33] Jeong J-H, Jo H, Laflamme S, et al. Automatic control of AC bridge-based capacitive strain sensor interface for wireless structural health monitoring. *Measurement*. Oct 2022;202:111789.
[34] Oliva PV, Wu Y, He C, et al. Towards fast weak adversarial training to solve high dimensional parabolic partial differential equations using XNODE-WAN. *J Comput Phys*. Aug 2022;463:111233.
[35] Hoang T, Fu Y, Mechitov K, et al. Autonomous end-to-end wireless monitoring system for railroad bridges. *Adv Bridge Eng*. Dec 2020;1.
[36] Fu Y, Hoang T, Mechitov K, et al. Sudden event monitoring of civil infrastructure using demand-based wireless smart sensors. *Sensors*. Dec 2018;18:4480.
[37] Fu Y, Mechitov K, Hoang T, et al. Development and full-scale validation of high-fidelity data acquisition on a next-generation wireless smart sensor platform. *Adv Struct Eng*. Aug 2019;22:3512–3533.
[38] Kong X, Li J, Collins W, et al. A large-area strain sensing technology for monitoring fatigue cracks in steel bridges. *Smart Mater Struct*. Jul 2017;26:085024.
[39] Kong X, Li J, Collins W, et al. Sensing distortion-induced fatigue cracks in steel bridges with capacitive skin sensor arrays. *Smart Mater Struct*. Oct 2018;27:115008.
[40] Kong X, Li J, Bennett C, et al. Thin-film sensor for fatigue crack sensing and monitoring in steel bridges under varying crack propagation rates and random traffic loads. *J Aerospace Eng*. Jan 2019;32.
[41] Cai L, Song L, Luan P, et al. Super-stretchable, transparent carbon nanotube-based capacitive strain sensors for human motion detection. *Sci Rep*. Oct 2013;3.
[42] Pasadas F, Jimenez D. Large-signal model of graphene field-effect transistors—part i: compact modeling of GFET intrinsic capacitances. *IEEE Trans Electron Dev*. Jul 2016;63(7):2936–2941.
[43] Lilly J, Olhede S. Higher-order properties of analytic wavelets. *IEEE Trans Signal Process*. Jan 2009;57(1):146–160.
[44] Aguiar-Conraria L, Soares MJ. The continuous wavelet transform: moving be-yond Uni- and bivariate analysis. *J Econ Surv*. Feb 2013;28:344–375.
[45] Aygun LE, Kumar V, Weaver C, et al. Large-area resistive strain sensing sheet for structural health monitoring. *Sensors*. Mar 2020;20:1386.
[46] Smith C, Downey AR. Additively manufactured flexible hybrid electronic sensor for discrete fatigue crack detection. In: *AIAA SCITECH 2023 Forum*. American Institute of Aeronautics and Astronautics; Jan 2023.
[47] Qiu L, Lin X, Wang Y, et al. A mechatronic smart skin of flight vehicle struc- tures for impact monitoring of light weight and low-power consumption. *Mech Syst Signal Process*. Oct 2020;144:106829.
[48] NextFlex. About flexible hybrid electronics: defining flexible hybrid electronics (FHE). 2022. https://www.nextflex.us/about/about-fhe/